Test cases description

The two test cases are taken from the ERCOFTAC Classic Database, [1]. The computational domains of the two selected test cases are very similar: the inlet and outlet boundaries are vertical lines with $x = constant$, the top boundary is a flat wall with $y = constant$ and the bottom boundary is also a wall, but with a more difficult shape.

1 Geometry of the test cases and flow conditions

1.1 Flow over a hill, C-18

The geometry of the test case is illustrated in figure (1), which is taken from [1].

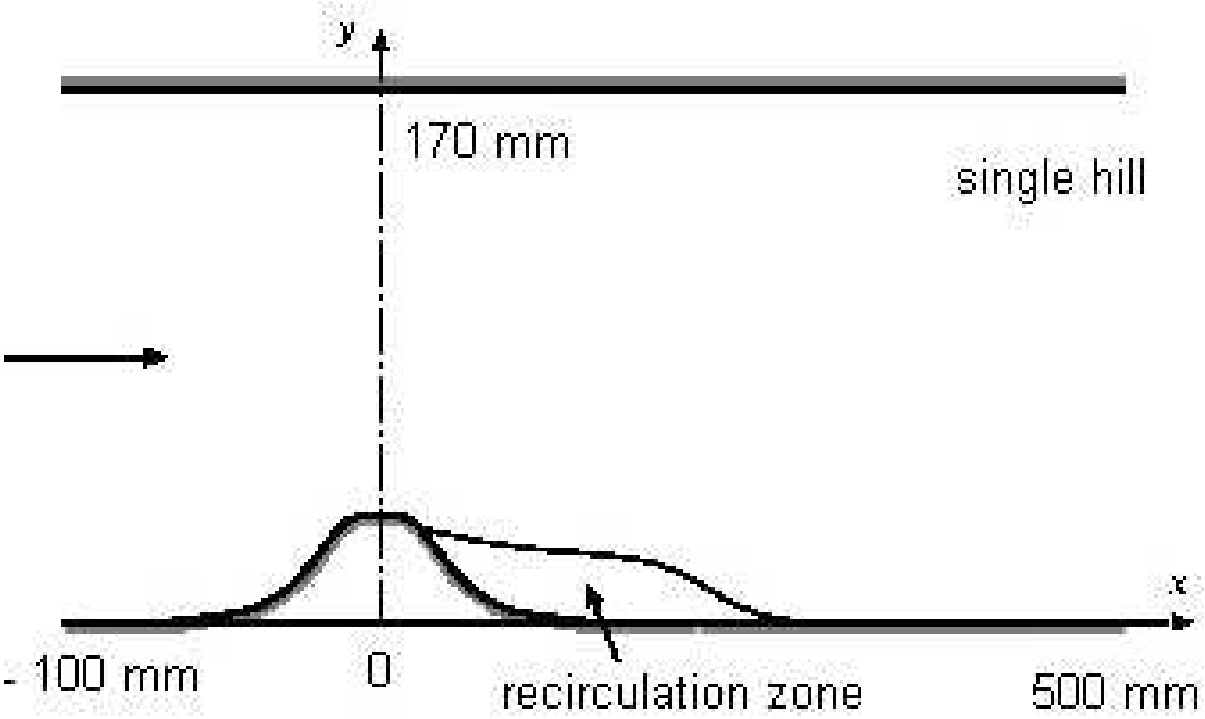

Figure 1: Geometry of the flow over a 2-D Hill.

The computational domain is bounded by two solid walls and the inlet and outlet boundaries, which means that there are only two boundaries with exact boundary conditions. The Reynolds number based on the hill height, $h = 28$mm, and on the mean centreline velocity at the inlet, $U_o = 2.147$m/s, is $R_n = 60000$.

The inlet boundary is an $x = constant$ line located at $x = -300$mm, i.e. $x \simeq -10.7h$ and the outlet boundary is an $x = constant$ line at $x = 800$mm $(x \simeq 28.6h)$. The maximum distance between the two walls is 170mm, i.e. approximately $6h$.

1.2 Flow over a backward facing step, C-30

The geometry of the experimental setup of this flow is depicted in figure (2), which is taken from [1].

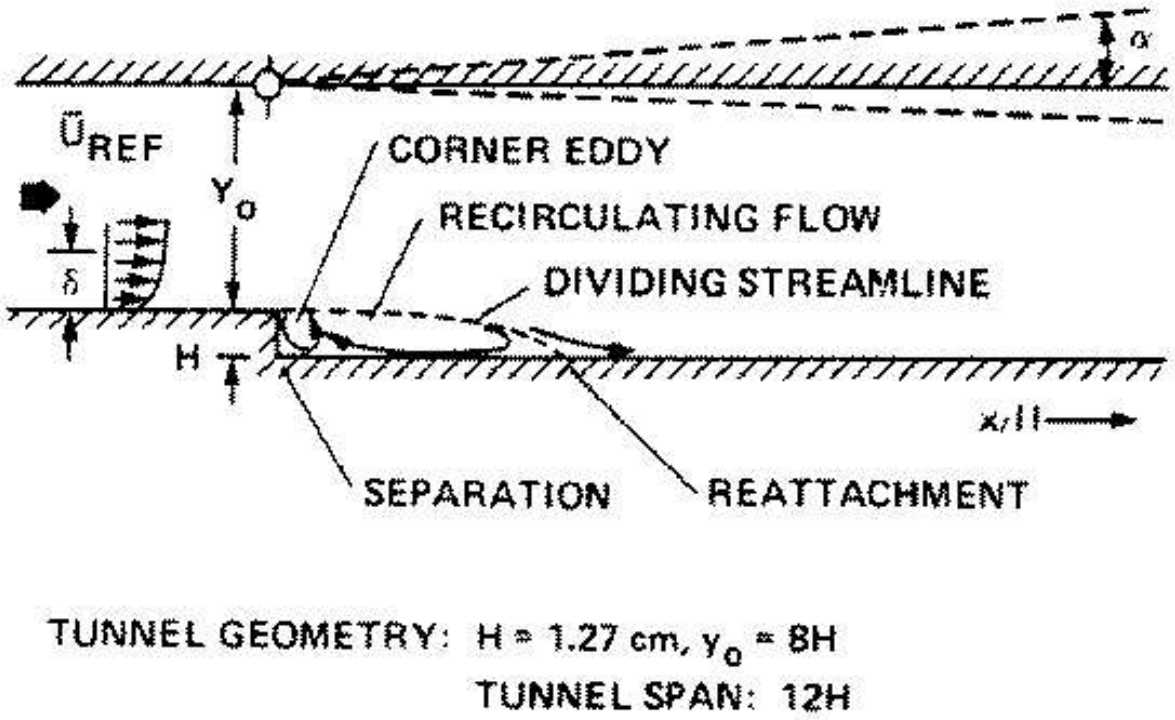

Figure 2: Geometry of the flow over a backward facing step.

In the present grid sets, the angle of the top wall is 0 degrees. The velocity of the uniform incoming flow, U_{ref}, is 44.2 m/s and the step height, h, is 1.27 cm. The inlet is an $x = constant$ section located 4 step heights upstream of the step and the outlet is an $x = constant$ section 40 step heights downstream of the step. The Reynolds number based on U_{ref} and h is 50000.

2 Grid Sets

In both cases, all the grid sets include single block structured grids. One family of grid lines connects the inlet and outlet boundaries, whereas the other family of grid lines runs between the top and bottom walls.

This choice may not lead to the optimal grid, but the main objective of the present grids is to allow its use with the maximum number of flow solvers possible, guaranteing that we have sets of geometrical similar grids. To achieve this result a basis grid is generated for each test case. Each grid is then obtained with a 2-D cubic spline interpolation performed on the basis grid. The desired grid line distance is obtained with 1-D coordinate transformations tuned at the inlet and bottom boundaries using the stretching functions proposed by Vinokur in [3].

The basis grids are generated with a package developed within the IST/MARIN cooperation, [2], which includes hyperbolic, elliptical and algebraic techniques.

2.1 Flow over a hill, C-18

The basis grid for the flow over the hill includes 595×201 grid nodes.

Figure (3) illustrates the basis grid. The view of the complete grid includes a reduced number of grid lines, whereas the detailed view in the vicinity of the hill includes all the grid lines.

Deviations from Orthogonality	Interior Nodes	Boundaries			
		Bottom wall	Top wall	Inlet	Outlet
Maximum (^{o})	0.26	1.69	0.01	0.00	0.00
Mean (^{o})	0.00	0.11	0.00	0.00	0.00

Table 1: Deviations from orthogonality of the basis grid for the flow over a hill.

The deviations from orthogonality are presented in table (1). In the interior grid nodes, the derivatives of the grid coordinates are approximated by central-differences. At the boundaries, the derivatives with respect to the curvilinear coordinate perpendicular to the boundary are approximated with one-sided first-order differences, whereas the derivative with respect to the curvilinear coordinate that changes along the boundary are also approximated by central-differences. The results of table (1) show that the grid is nearly-orthogonal.

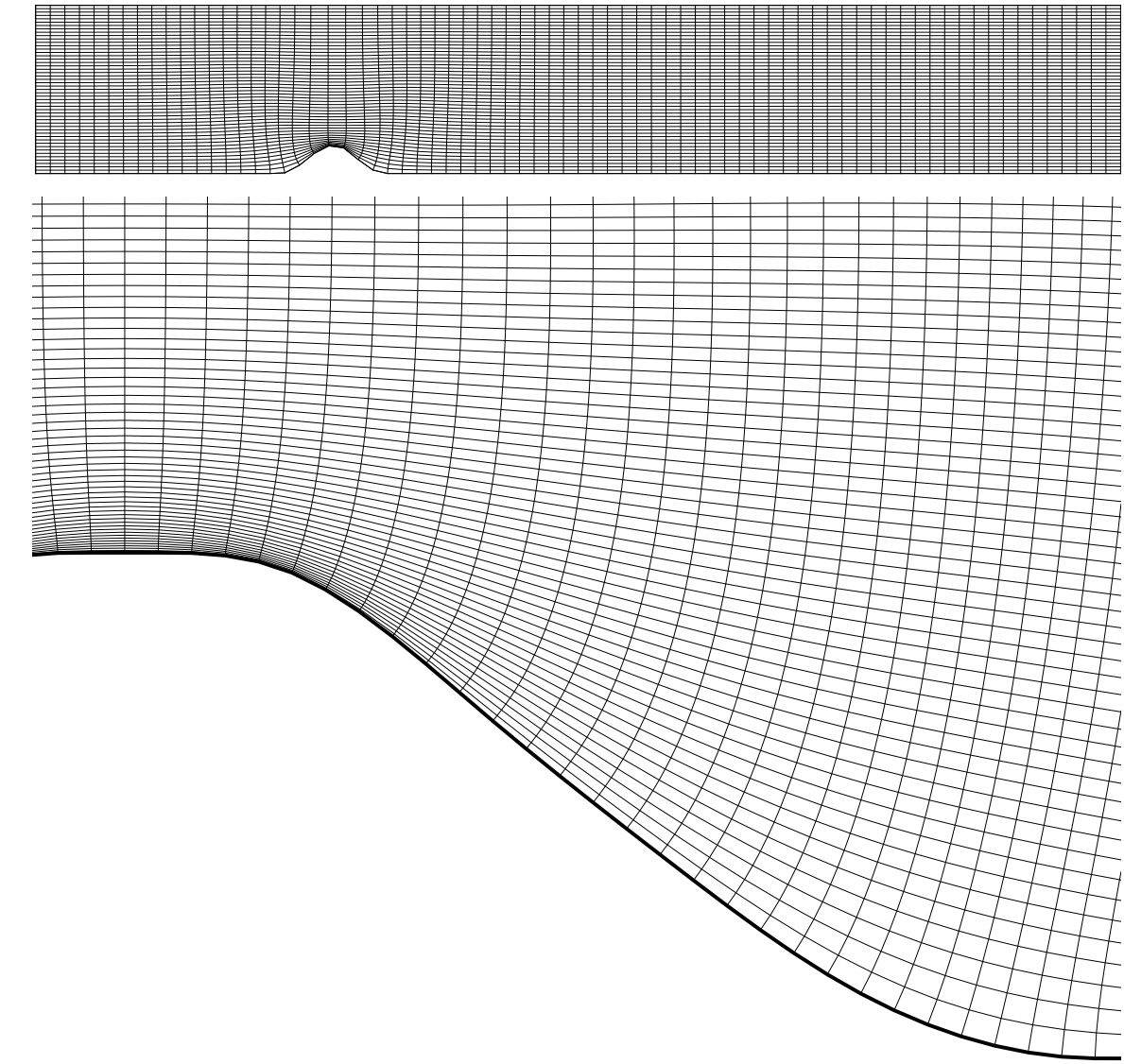

Figure 3: Basis grid for the flow over a 2-D Hill.

2.1.1 Grid set A

Grid set A is composed of 11 geometrically similar grids that preserve the grid line pattern of the original basis grid. The grids have an equal number of grid nodes in both directions, $N_\xi = N_\eta$. The near-wall grid line distances were selected to enable a proper application of the no-slip condition. The typical values of the maximum y^+ at the first grid node away from the walls, $(y_2^+)_{max}$, are given in table (2).

Figure (4) presents a view of the 101×101 grid of set A close to the hill.

Typical	N_ξ or N_η										
$(y_2^+)_{max}$	101	121	141	161	181	201	241	281	321	361	401
Top	0.77	0.64	0.55	0.48	0.43	0.39	0.32	0.28	0.24	0.21	0.19
Bottom	0.71	0.59	0.51	0.44	0.39	0.36	0.30	0.26	0.22	0.20	0.18

Table 2: Maximum value of y^+ at the first grid node away from the walls in grid set A. Flow over a hill.

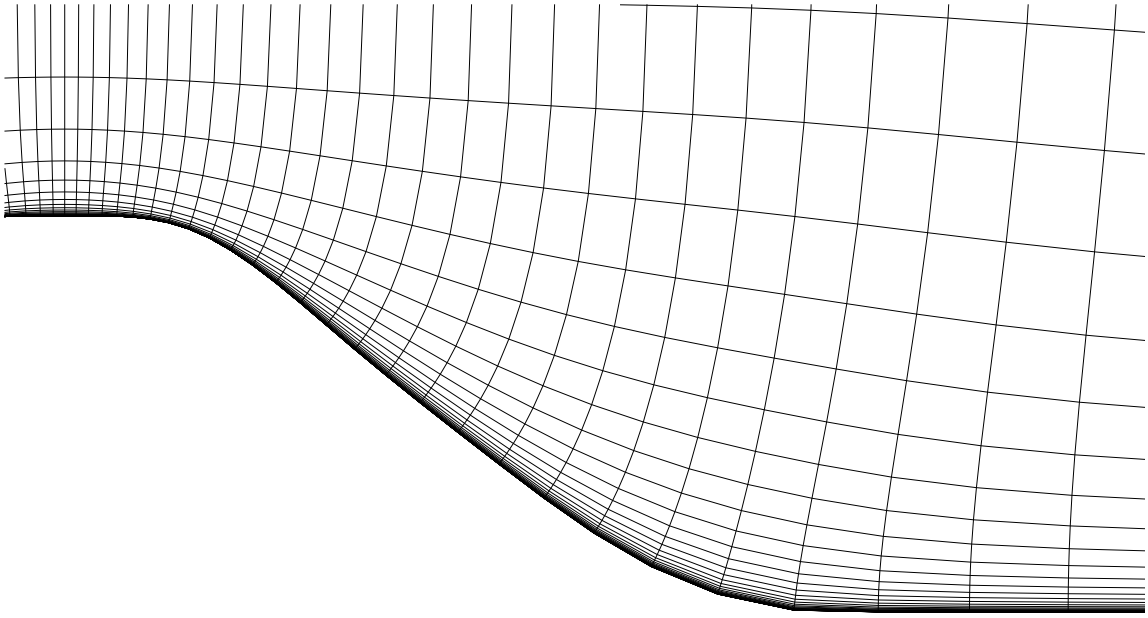

Figure 4: 101×101 grid of set A for the flow over a 2-D Hill.

2.1.2 Grid set B

The grids of set B are straightforward to generate. In this set, the η lines have a constant x coordinate, which is taken from the boundary point distribution at the bottom boundary in set A. The grid node distribution along these normal lines is defined by the stretching function applied at the inlet boundary of set A. Therefore, the grids still have smooth ξ lines, but we no longer have nearly-orthogonal grids.

In the grids of set B, the mean deviation from orthogonality in the interior is 5.4^o and the maximum deviation is 40.5^o. The grids are orthogonal at the inlet, outlet and top boundaries, but there is a significant deviation from orthogonality at the bottom wall, with a maximum deviation from orthogonality of 40.5^o in the hill region.

The values of $(y_2^+)_{max}$ in this grid set are given in table (5.3).

Typical	N_ξ or N_η										
$(y_2^+)_{max}$	101	121	141	161	181	201	241	281	321	361	401
Top	0.78	0.65	0.55	0.49	0.43	0.39	0.32	0.28	0.24	0.22	0.19
Bottom	1.34	1.12	0.96	0.84	0.75	0.67	0.56	0.48	0.42	0.38	0.34

Table 3: Maximum value of y^+ at the first grid node away from the walls in grid set B. Flow over a hill.

The 101×101 grid is illustrated in figure (5).

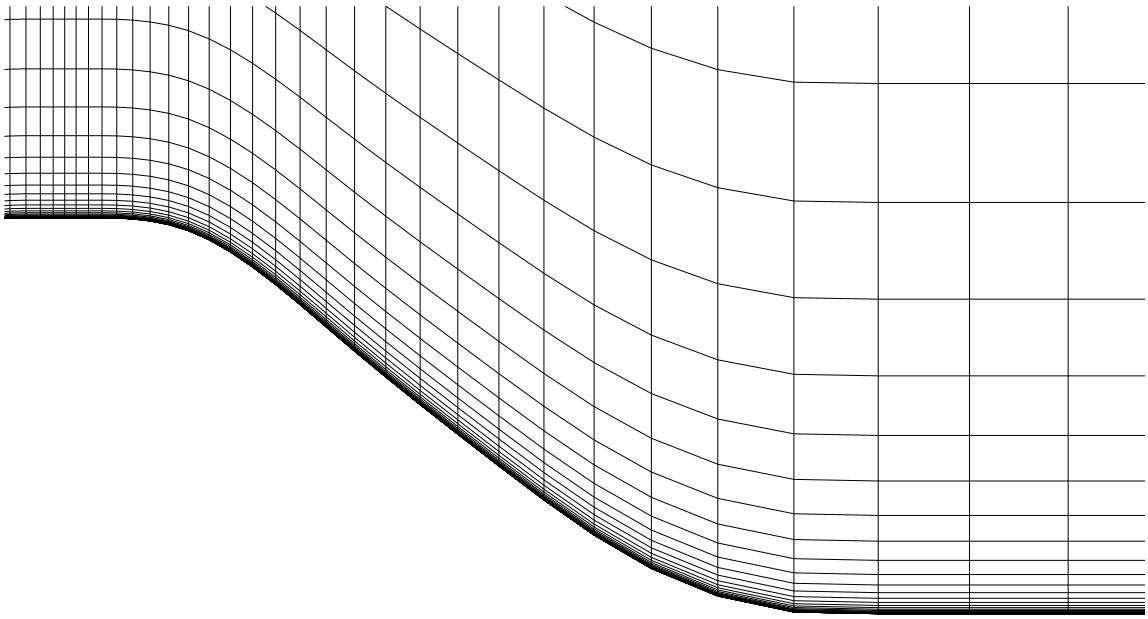

Figure 5: 101×101 grid of set B for the flow over a 2-D Hill.

2.2 Flow over a backward facing step, C-30

The choice of a single block, structured grid for the present computational domain makes the grid generation a challenging task. The two corners of the bottom wall are not easy to handle in such a grid. It is obvious that it is possible to generate much simpler grids using different topologies than the present choice. A simple example is a multiblock Cartesian grid. However, one of the goals of the present exercise is to test the reliability of the uncertainty estimates in

difficult situations and so the single block structured grid is a really demanding test case for any flow solver.

The basis grid has 321×321 grid nodes and we have ensured that the two corners of the step are coincident with grid nodes.

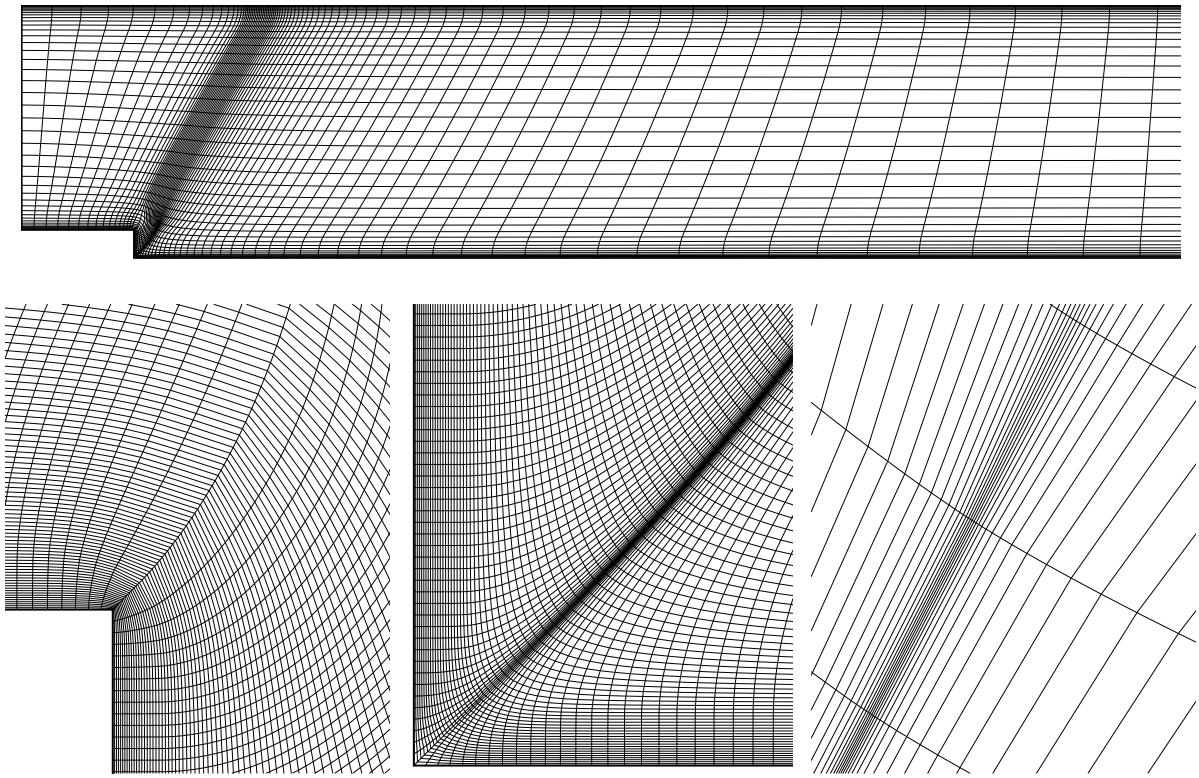

Figure 6: Basis grid for the flow over a 2-D backward facing step.

Figure (6) illustrates the basis grid. The view of the complete grid includes a reduced number of grid lines, whereas the detailed views in the vicinity of the step include all the grid lines. The consequences of the two corners of the bottom boundary in the interior grid line spacing are perfectly visible in the grid plots.

Obviously, the deviations from orthogonality are much larger than in the previous test case. Nevertheless, the values obtained are still acceptable and most of the times common practice in complex configurations. Table (4) presents the mean and maximum deviations from orthogonality of the basis grid in the interior grid nodes and at the four boundaries of the computational domain. These values were computed with the same discretization schemes applied in the previous test case.

Deviations from Orthogonality	Interior Nodes	Boundaries			
		Bottom wall	Top wall	Inlet	Outlet
Maximum (^{o})	43.3	31.6	0.00	0.78	0.49
Mean (^{o})	14.6	0.52	0.00	0.28	0.17

Table 4: Deviations from orthogonality of the basis grid for the flow over a backward facing step.

2.2.1 Grid set A

This grid set is obtained with 2-D cubic splines interpolations in the basis grid, which are similar to the technique applied in grid set A of the flow over the hill. In this case, the interpolation is performed in three sub-domains to take into account the discontinuities of the coordinates derivatives at the two corners of the bottom wall. In this grid set, there is always a grid node at the two corners of the step.

The boundary node distributions at the inlet boundary and at the bottom wall are specified using the stretching functions proposed by Vinokur, [3]. At the bottom wall, we have adopted an equidistant node distribution along the vertical wall of the step. In each grid, one fifth of the grid nodes are located between the inlet and the top corner of the step. Another fifth is used along the vertical line of the step and the remaining three fifths are placed between the bottom corner and the outlet of the computational domain. At the inlet boundary, a two-sided stretching function is applied to obtain the required near-wall spacing.

7 geometrically similar grids have been generated with the values of $(y_2^+)_{max}$ given in table (5).

Typical $(y_2^+)_{max}$	N_ξ or N_η						
	101	121	141	161	181	201	241
Top	0.89	0.71	0.60	0.52	0.46	0.41	0.34
Bottom	1.01	0.82	0.68	0.58	0.55	0.44	0.36

Table 5: Maximum value of y^+ at the first grid node away from the walls in grid set A. Flow over a backward facing step.

Figure (7) presents three views of the 101×101 grid.

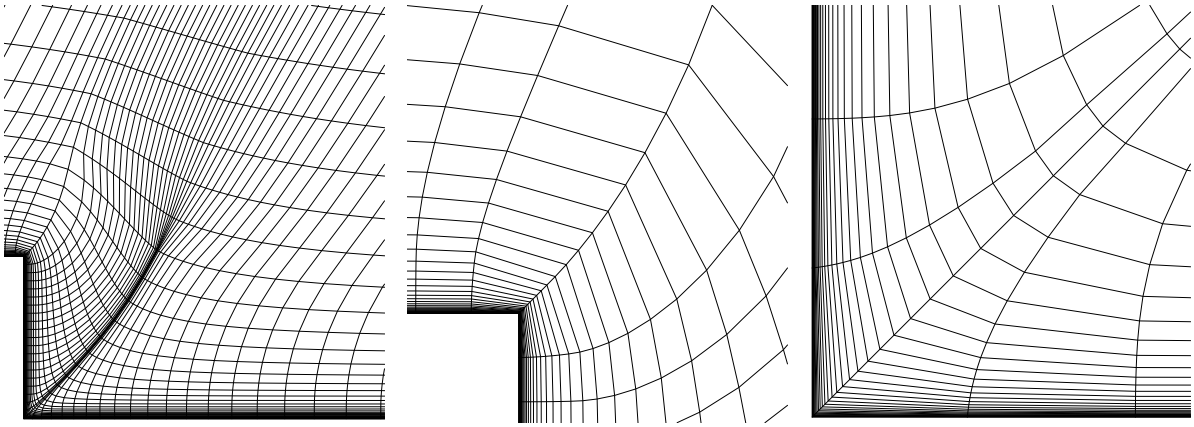

Figure 7: 101×101 grid of set A for the flow over a backward facing step.

2.2.2 Grid set B

The 7 grids of set B have the same boundary point distribution of the corresponding grid of set A. However, in this case the interior grid lines are obtained simply by connecting the grid nodes of the top and bottom walls with straight lines. The two-sided stretching function at the inlet is applied to all the η lines of each grid to obtain the desired interior grid line spacing.

Deviations from Orthogonality	Interior Nodes	Boundaries			
		Bottom wall	Top wall	Inlet	Outlet
Maximum (^{o})	63.3	63.3	29.1	0.64	0.00
Mean (^{o})	25.6	29.8	23.5	2.74	0.00

Table 6: Deviations from orthogonality of the grids of set B for the flow over a backward facing step.

Table (6) presents the mean and maximum deviations from orthogonality of the grids of set B. The mean and maximum deviations from orthogonality are clearly larger than in the basis grid. Furthermore, at the two solid walls the grid lines are clearly non-orthogonal.

Typical $(y_2^+)_{max}$	N_ξ or N_η						
	101	121	141	161	181	201	241
Top	0.93	0.75	0.62	0.54	0.47	0.42	0.34
Bottom	1.15	0.93	0.78	0.67	0.58	0.52	0.42

Table 7: Maximum value of y^+ at the first grid node away from the walls in grid set B. Flow over a backward facing step.

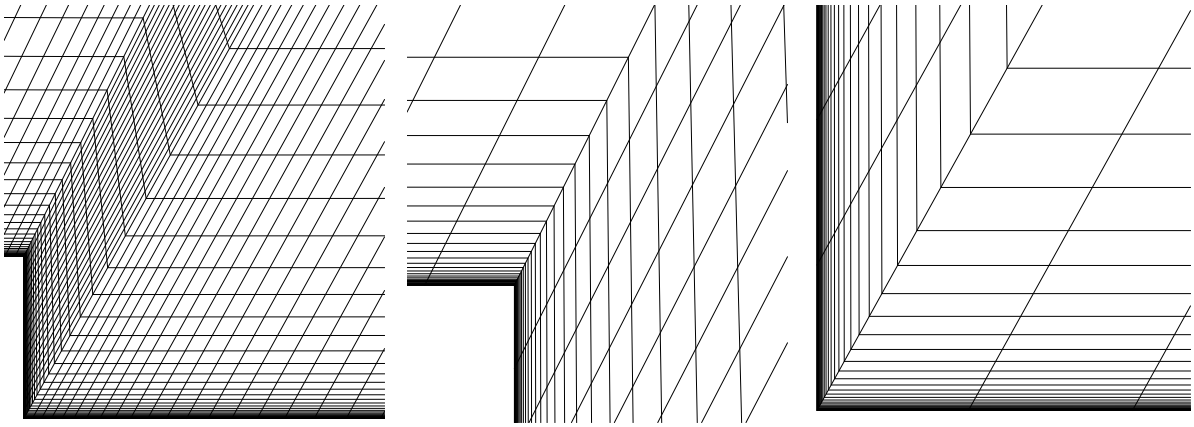

Figure 8: 101×101 grid of set B for the flow over a backward facing step.

The typical values of $(y_2^+)_{max}$ are presented in table (7). Figure (8) illustrates the 101×101 grid of set B.

2.2.3 Grid set C

In practical applications, it may be impossible to guarantee the existence of a grid node at every corner of a complex configuration. Therefore, we have generated a third grid set which does not have grid nodes coincident with the two corners of the step. The grids are generated in a similar way of grid set A and so we have grid properties which are not too different from the ones of the basis grid.

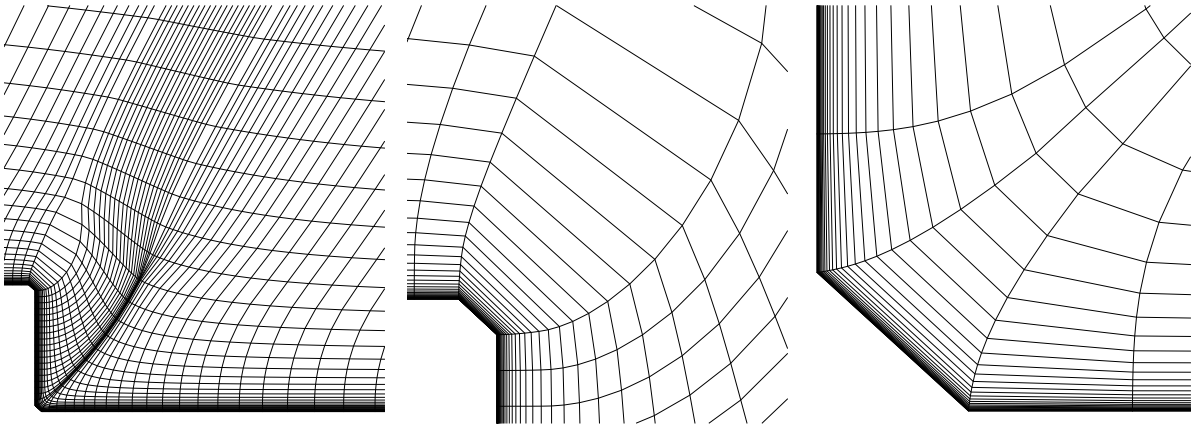

Figure 9: 101×101 grid of set C for the flow over a backward facing step.

The stretching function applied in the η direction is the same as in set A and so the values of $(y_2^+)_{max}$ given in table (5) are very similar to the ones obtained in grid set C.

Figure (9) presents three views of the 101×101 grid of set C.

3 Inlet Profiles

In both test cases there are no exact boundary conditions available at the inlet boundary. Therefore, some approximations have to be made for the specification of the inlet boundary conditions.

3.1 U^1 Velocity component

The Cartesian velocity component in the x direction, U^1, is defined with the help of analytical profiles. The present options were tuned to obtain a good agreement with the experimental results. The U^1 profile in the vicinity of the two walls is assumed to be identical and so one only needs to specified it for half the distance between the two walls.

3.1.1 Flow over a hill

In this case, the mean centreline velocity is designated by U_o and half the distance between the two walls by H_2. The inlet U^1 profile is defined with a multi-layer approach:

- For $y^+ < 100$:

$$U^+ = \frac{1}{\kappa}\ln\left(1+0.4y_n^+\right) + 7.8\left(1 - e^{-\frac{y_n^+}{11}} - \frac{y_n^+}{11}e^{-\frac{y_n^+}{3}}\right) , \tag{1}$$

where

$$U^+ = \frac{U^1}{u_\tau} \text{ and } \kappa = 0.41 .$$

Equation (1) is given in [4] and it is based on a compilation of Direct Numerical Simulation and Large Eddy-Simulation data. u_τ was set equal to the experimental value $u_\tau = 0.079$m/s.

- For $y^+ \geq 100$ and $y < 0.6H_2$:

$$\frac{U^1}{U_o} = \left(\frac{y}{H_2}\right)^\gamma , \tag{2}$$

where the exponent γ is obtained from the continuity of equations (1) and (2) at $y^+ = 100$.

- For $y \geq 0.6H_2$:

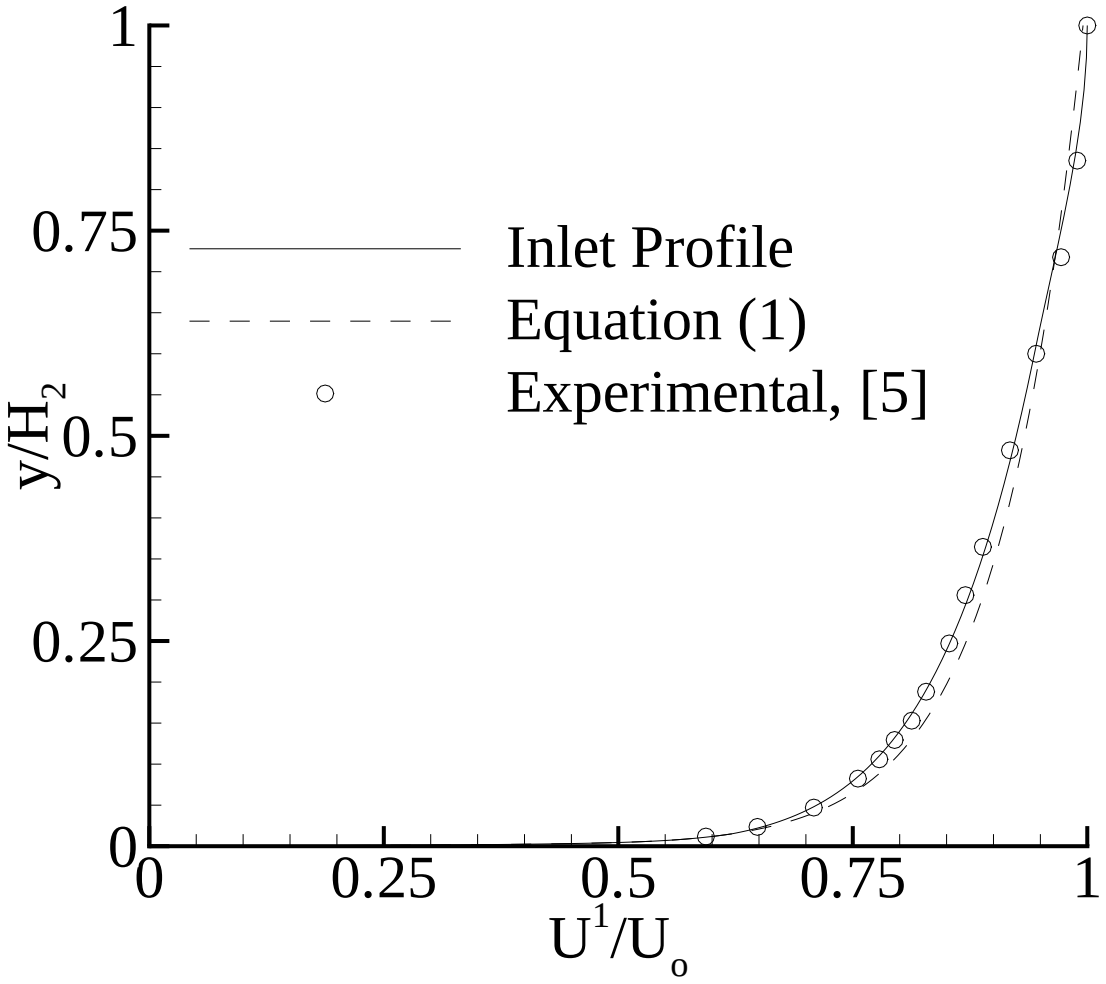

Figure 10: Inlet U^1 profile for the steady, incompressible, 2-D flow over a hill.

The velocity profile is obtained with an Hermite interpolation. The derivative with respect to y at $0.6H_2$ is obtained from equation (2) and at H_2 is set equal to zero.

Figure (10) presents the inlet velocity profile and the experimental results, [5]. The profile obtained from equation (1) is also plotted in figure (10).

3.1.2 Backward facing step

In the experimental setup of this flow there is a uniform flow at the inlet with boundary-layer type profiles close to the two walls.

The inlet conditions are given in [6] four step-heights upstream of the step, which has a height, h, of 1.27cm. At this location, the boundary-layer thickness, δ, is 1.9cm and the

Reynolds number based on the inlet velocity, U_{ref}, and on the momentum thickness, θ, is

$$Re_\theta = \frac{U_{ref}\theta}{\nu} = 5000.$$

The boundary-layer region is represented with a similar strategy to the one used in the flow over a hill. The U^1 profile is specified with a three layer approach.

- For $y^+ < 25$:

A standard boundary-layer profile described in [7], which is defined from the momentum thickness and the skin friction coefficient, C_f. θ and C_f were selected to obtain the best agreement with the experimental data.

$$\frac{\theta}{h} = 0.15 \text{ and } C_f = 0.003\,.$$

With these choices of θ and C_f one obtains $\delta = 1.99h$ at the inlet boundary.

- For $y^+ \geq 25$ and $y < 0.3\delta$:

$$\frac{U^1}{U_{ref}} = \left(\frac{y}{\delta}\right)^\gamma, \tag{3}$$

where the exponent γ is obtained from the continuity of the U^1 profile at $y^+ = 25$.

- For $y \geq 0.3\delta$:

The velocity profile is obtained with an Hermite interpolation. The derivative with respect to y at 0.3δ is obtained from the power-law profile and at δ is set equal to zero.

Figure (11) presents the inlet velocity profile and the experimental results, [6]. The standard boundary-layer profile suggested in [7] is also plotted in figure (11).

3.2 Turbulent quantities

The selected inlet boundary conditions lead always to the same eddy-viscosity profile, independently of the turbulence model chosen. k and ε approximate inlet profiles are defined and the ν_t profile is obtained using Chien's $k-\varepsilon$ model, [8]. The remaining variables, $(\tilde{\nu})_t$, $\tilde{\nu}$ and ω are derived from the others.

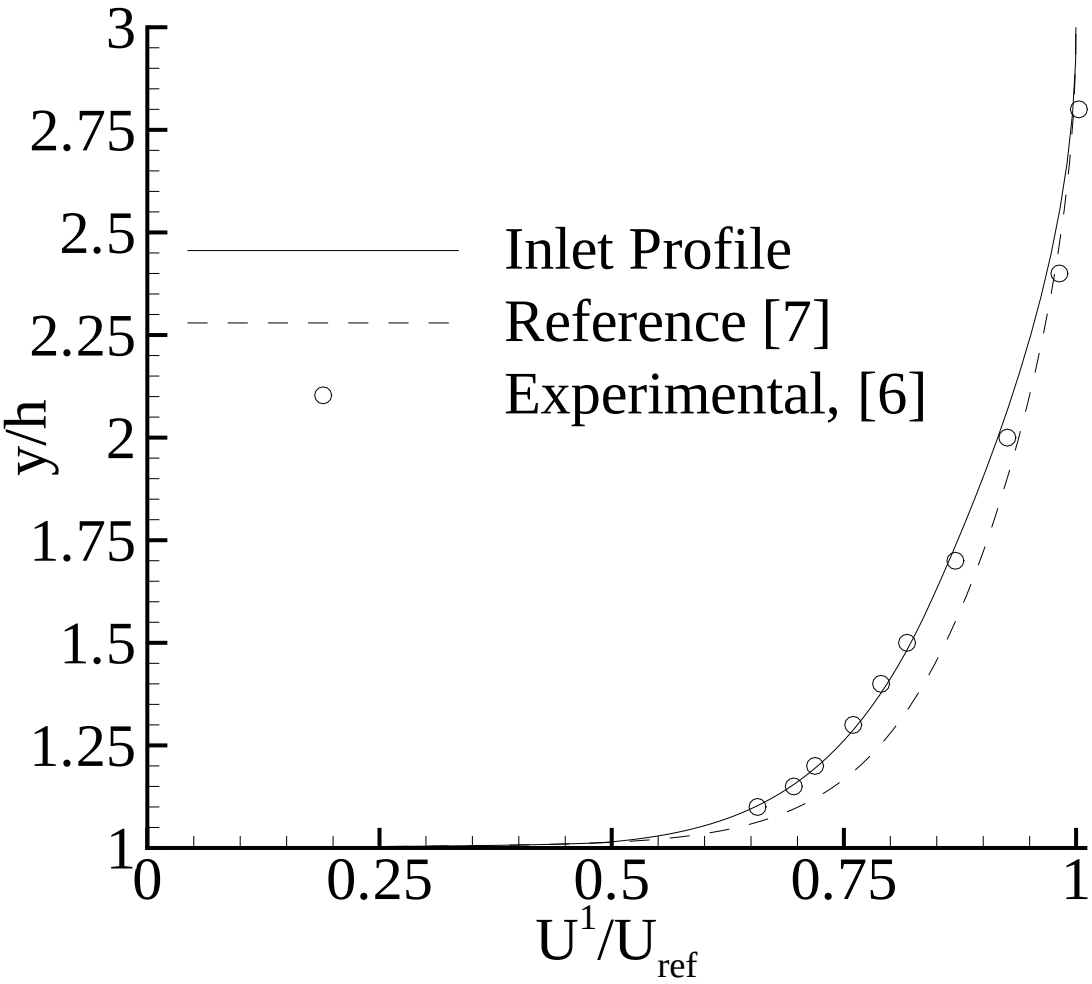

Figure 11: Inlet U^1 profile for the steady, incompressible, 2-D flow over a backward facing step.

3.2.1 Flow over a hill

The inlet boundary k and ε profiles are specified with equations given in [4]. The k profile is given by

$$k^+ = 0.07(y^+)^2 e^{-\frac{y^+}{8}} + 4.5\left(1 - e^{-\frac{y^+}{20}}\right)\frac{1}{\frac{4y^+}{Re_{u_\tau}} + 1}\,, \tag{4}$$

where

$$k^+ = \frac{k}{u_\tau^2} \text{ and } Re_{u_\tau} = \frac{u_\tau h}{\nu}\,.$$

h is the hill height.

ε is obtained from

$$\varepsilon^+ = \frac{1}{0.41\left((y^+)^4 + 15^4\right)^{0.25}} , \tag{5}$$

with

$$\varepsilon^+ = \frac{\varepsilon \nu}{u_\tau^4} .$$

3.2.2 Backward facing step

In the backward facing step k has a constant value in the uniform flow region and a multi-layer profile in the near-wall region.

In the uniform flow region, the turbulent quantities are selected to obtain an eddy-viscosity equal to 0.01ν. Of the three turbulent quantities, k, ε and ω, the value of ω is known to be the most sensitive. Therefore, k and ε are obtained as a consequence of the selected values of eddy-viscosity and ω.

In the boundary-layer region the multi-layer profile is given by:

$$\begin{array}{rcll} k^+ &=& 0.05(y_n^+)^2 & \Leftarrow \quad y_n^+ < 5 \\ k^+ &=& 1.25 + 0.325(y_n^+ - 5) & \Leftarrow \quad 5 \le y_n^+ < 15 \\ k^+ &=& 4.5 - 3.6\eta^2 + 2.4\eta^3 \text{ with } \eta = \frac{y_n^+ - 15}{45} & \Leftarrow \quad 15 \le y_n^+ < 60 \\ k^+ &=& 3.3 & \Leftarrow \quad 60 \le y_n^+ \text{ and } y_n < 0.15\delta \end{array} \tag{6}$$

A cubic interpolation is applied between $y_n = 0.15\delta$ and the edge of the boundary layer using zero derivatives at $y_n = 0.15\delta$ and $y_n = \delta$.

For $y \ge \delta$,

$$k = \frac{0.1}{R_n} U_{ref}^2 ,$$

where R_n is the Reynolds number, given by $R_n = \frac{U_{ref} h}{\nu}$.

ε is defined with different equations for the near-wall region and for the outer region of the boundary-layer. For $y_n < 0.15\delta$, ε is obtained from

$$\varepsilon = \frac{k^{1.5}}{l} , \tag{7}$$

with

$$l = 2.543687 y_n \left(1 - e^{-R_k/5.087374}\right) \tag{8}$$

and

$$R_k = \frac{\sqrt{k} l}{\nu} . \tag{9}$$

In the outer region ε is obtained with an Hermite interpolation for the region $0.15\delta < y_n < \delta$. The derivative at $y = \delta$ is set equal to zero and the derivative at 0.15δ is obtained from the linear variation between 0.15δ and δ.

For $y \geq \delta$,

$$\varepsilon = \frac{0.09}{R_n} \frac{U_{ref}^3}{h} .$$

In both cases, $\tilde{\varepsilon}$ for Chien's model is obtained from

$$\tilde{\varepsilon} = \max\left(0, \varepsilon - \frac{2\nu k}{y_n^2}\right) .$$

The ν_t profile is computed with Chien's $k-\varepsilon$ model. $(\tilde{\nu})_t$ and $\tilde{\nu}$ are obtained solving the non-linear problems defined by the definition equation of the eddy-viscosity in the one-equation models of Spalart & Allmaras, [9], and [10].

The ω profile is specified with the help of the k and ν_t profiles with the exception of the near-wall viscous sub-layer.

$$\begin{aligned} \omega &= \frac{6\nu}{0.075 y_n^2} \quad y_n^+ < 2.5 \\ \omega &= \frac{k}{\nu_t} \quad 2.5 \leq y_n^+ \text{ and } 0.15\delta \\ \omega &= 10\frac{U_{ref}}{h} \quad y_n > \delta \end{aligned} \tag{10}$$

References

[1] ERCOFTAC Classic Collection Database - http://cfd.me.umist.ac.uk/ercoftac

[2] Eça L. - *Grid Generation Tools for Structured Grids.* - IST Report D72-18, Instituto Superior Técnico, Lisbon, May 2003.

[3] Vinokur M. - *On One-Dimensional Stretching Functions for Finite-Difference Calculations.* - Journal of Computational Physics, Vol. 50, 1983, pp. 215-234.

[4] Davroux A., Hoa C., Laurence D. - *Flow Over a 2D Hill: Reference Solutions for $k-\varepsilon$ and Second Moment Closure Turbulence Models* - http://cfd.me.umist.ac.uk/ercoftac/database/cases/case18/Case_rsoln/hillpap.html

[5] Almeida G.P., Durão D.F.G., Heitor M.V. - *Wake Flows behind Two-dimensional Model Hills* - Experimental Thermal and Fluid Science, 7, p. 81, 1992.

[6] Driver D.M., Seegmiller H.L. - *Features of a Reattaching Turbulent Shear Layer in Divergent Channel Flow* - AIAA Journal, Vol. 23, N. 2, February 1985.

[7] Hoekstra M. - *Generation of Initial Velocity Profiles for Boundary Layer Calculations* - Marin Report Nº 50028-1-SR, March 1980.

[8] Chien K.Y - *Prediction of Channel and Boundary-Layer Flows with a Low-Reynolds-Number Turbulence Model.* - AIAA Journal, January 1992, pp. 33-38.

[9] Spalart P.R., Allmaras S.R. - *A One-Equations Turbulence Model for Aerodynamic Flows* - AIAA 30th Aerospace Sciences Meeting, Reno, January 1992.

[10] Menter F.R. - *Eddy Viscosity Transport Equations and Their Relation to the $k-\varepsilon$ Model* - Journal of Fluids Engineering, Vol. 119, December 1997, pp. 876-884.